Pure Appl. Geophys. 173 (2016), 333–348

DOI 10.1007/s00024-015-1225-4

Pure and Applied Geophysics

The 16 September 2015 Chile Tsunami from the Post-Tsunami Survey and Numerical Modeling Perspectives

Rafael Aránguiz,[1,2] Gabriel González,[2,3] Juan González,[2,3] Patricio A. Catalán,[2,4,5] Rodrigo Cienfuegos,[2,6] Yuji Yagi,[7] Ryo Okuwaki,[8] Luisa Urra,[1] Karla Contreras,[1] Ian Del Rio,[2,3] and Camilo Rojas[3]

Abstract—On September 16, 2015 a magnitude Mw 8.3 earthquake took place off the coast of the Coquimbo Region, Chile. Three tsunami survey teams covered approximately 700 km of the Pacific coast. The teams surveyed the area, recording 83 tsunami flow depth and runup measurements. The maximum runup was found to be 10.8 m at only one small bay, in front of the inferred tsunami source area. However, it was observed that runup in other locations rarely exceed 6 m. Tsunami runup was larger than those of the 2014 Pisagua event, despite the similar earthquake magnitude. Moreover, tsunami arrival times were found to be shorter than those of previous tsunamis along the Chilean subduction zone. Numerical simulations of the tsunami event showed a good agreement with field data, highlighting that tsunami arrival time and the spatial variation of the tsunami amplitudes were strongly influenced by the bathymetry, coastal morphology and the slip distribution of the causative earthquake.

Key words: Tsunami, chile, runup, continental shelf, south pacific ocean.

1. Introduction

On September 16, 2015, at 22:54:33 UTC (19:54:33 local time) a magnitude Mw 8.3 earthquake took place off the coast of the Talinay Peninsula in the Coquimbo Region, Chile. The epicenter was located at 31.570°S, 71.670°W (Ye *et al*. 2015) with a focal depth of 23.3 km (http://www.sismologia.cl/), 37 km Northwest of Los Vilos. The 2015 Illapel Earthquake triggered a tsunami that reached the nearest coastal areas very fast, within few minutes of the earthquake initiation (some eyewitnesses suggest the tsunami started immediately after the earthquake at one coastal village). A tsunami threat message from the PTWC was issued 7 min after the main shock and the National Hydrographic and Oceanic Service (SHOA), the organization in charge of the Chile's National Tsunami Warning System, issued a tsunami alarm message 8 min after the earthquake (SHOA 2015a). A preventive evacuation status for the entire Chilean Coast was declared by the National Emergency Office (ONEMI) 11 min after the earthquake (ONEMI 2015). Despite the prompt evacuation, eight causalities were attributed to the tsunami (ONEMI 2015).

The last significant subduction earthquake in the area of the 2015 Illapel earthquake occurred in April 1943. The magnitude estimated for the 1943 earthquake was Mw 8.3 (Lomnitz 1970) with a total rupture length of 150–250 km (Nishenko 1985). That earthquake caused a minor tsunami, which mainly impacted Los Vilos (31.912°S, 71.513°W, south of the 2015 rupture area), where it damaged fishing boats (Lomnitz 1970; Soloviev and Go 1975). North of the location of the 2015 Illapel event, a large

This paper is part of the article collection on "Illapel, Chile, Earthquake on September 16th, 2015".

Electronic supplementary material The online version of this article (doi:10.1007/s00024-015-1225-4) contains supplementary material, which is available to authorized users.

[1] Department of Civil Engineering, Universidad Católica Ssma Concepción, Concepción, Chile. E-mail: raranguiz@ucsc.cl

[2] National Research Center for Integrated Natural Disaster Management CONICYT/FONDAP/1511007 (CIGIDEN), Santiago, Chile.

[3] Departamento de Ciencias Geológicas, Universidad Católica del Norte, Antofagasta, Chile.

[4] Departamento de Obras Civiles, Universidad Tecnica Federico Santa Maria, Valparaíso, Chile.

[5] Centro Científico Tecnológico de Valparaíso (CCTVal), Valparaíso, Chile.

[6] Departamento de Ingeniería Hidráulica y Ambiental, Pontificia Universidad Católica de Chile, Santiago, Chile.

[7] Faculty of Life and Environmental Sciences, University of Tsukuba, Tsukuba, Japan.

[8] Graduate School of Life and Environmental Sciences, University of Tsukuba, Tsukuba, Japan.

subduction earthquake in 1922 activated the adjacent segment of the megathrust. This earthquake had an estimated moment magnitude of 8.4 (Lomnitz 1970) and generated tsunami waves of 7–9 m in neighboring areas (Soloviev and Go 1975).

In this paper, we report the result of a post tsunami survey, which was conducted shortly after the earthquake, between September 21 and 28, 2015. We covered approximately 700 km of the Pacific coast between Chañaral (26.32°S) and Valparaiso (33.05°S). To understand the variation of the tsunami parameters along the coast, we also carried out tsunami numerical simulations. First we give a brief description of the bathymetry and coastal morphology, and then we present the tide gages records along the Chilean coast as well as the results of the post tsunami survey. The tsunami numerical simulation is presented in "Numerical Simulation". Then, we present a discussion and final conclusions.

2. Bathymetry and Coastal Morphology

The bathymetric structure of the sea bottom and the coastal morphology of the Coquimbo Region are fundamental to explaining the variation along the coast of the surveyed tsunami parameters. We provide a brief description of these two elements in this section.

The coast of the Coquimbo Region (29.832°S) shows two contrasting morphologies. From south of Punta Teatinos (29.821°S) to the northernmost tip of the Talinay Peninsula (Punta Lengua de Vaca, 30.317°S), the coast is characterized by three major bays: Coquimbo Bay, Guanaqueros Bay and Tongoy Bay (Fig. 1b). These bays open to the northwest, providing natural protection against predominant south-west swells, and are characterized by a lowland topography with long sandy beaches. Typically, these beaches exhibit seaward-concave plans typical of beaches on the leeside of a barrier or peninsula. The submarine part of these bays shows a nearly 10 km-wide marine platform with a gently sloping sea bottom. In particular, Coquimbo Bay shows depths that do not exceed 50 m within the bay. In contrast, the coast south of Talinay Peninsula is dominated by abrupt coastal cliff morphology extending southward to San Antonio. Several smaller bays are present, with the exception of Los Vilos, Quintero, Concon and Valparaiso, which are comparable in size to those in the Coquimbo area. In this southern segment, the marine platform is poorly developed and the bathymetry is dominated by isobaths deeper than 1000 m a short distance from the coastline (Fig. 1a). Along this segment some small beaches exist at the outlet of small creeks, where fishing villages are located. The inset in Fig. 1 shows the epicenter of the earthquake and a preliminary slip distribution done in the context of this work using 43 vertical component of teleseismic P-waveforms (Figure S1) downloaded through the Incorporated Research Institutions for Seismology Data Management Center (IRIS-DMC). The slip distribution model is constructed with the kinematic waveform inversion method developed by Yagi and Fukahata (2011). A beneficial aspect of this method is that the formulation takes into account the uncertainty in Green's function, which had been the major source of modeling errors in waveform inversion methods.

3. Tide Gages Data Analysis

Tsunami waves were instrumentally recorded by all tide gages along the Chilean coast (www.ioc-sealevelmonitoring.org), and the DART network across the Pacific Ocean. Figure 2 shows the tide gage records in Chile at the tide stations from 25°S to 36°S (Fig. 1a). The tide gage records show that the earthquake took place shortly after low tide near the epicenter (Fig. 2), meaning that maximum observed tsunami waves arrived during the flood tide. The tsunami arrived in Pichidangui, the tidegage closest to the main rupture patch, in less than 15 min. However, the maximum amplitudes did not exceed 2 m during first arrival. The arrival time at Coquimbo, located just north of the main rupture patch, occurred 23 min after the earthquake and peaked for first time 30 min after the earthquake, with 1.1 m of tsunami amplitude. This initial wave was followed by a succession of larger tsunami waves over a time span of 150 min. The maximum tsunami amplitude (4.75 m) was measured with the fourth

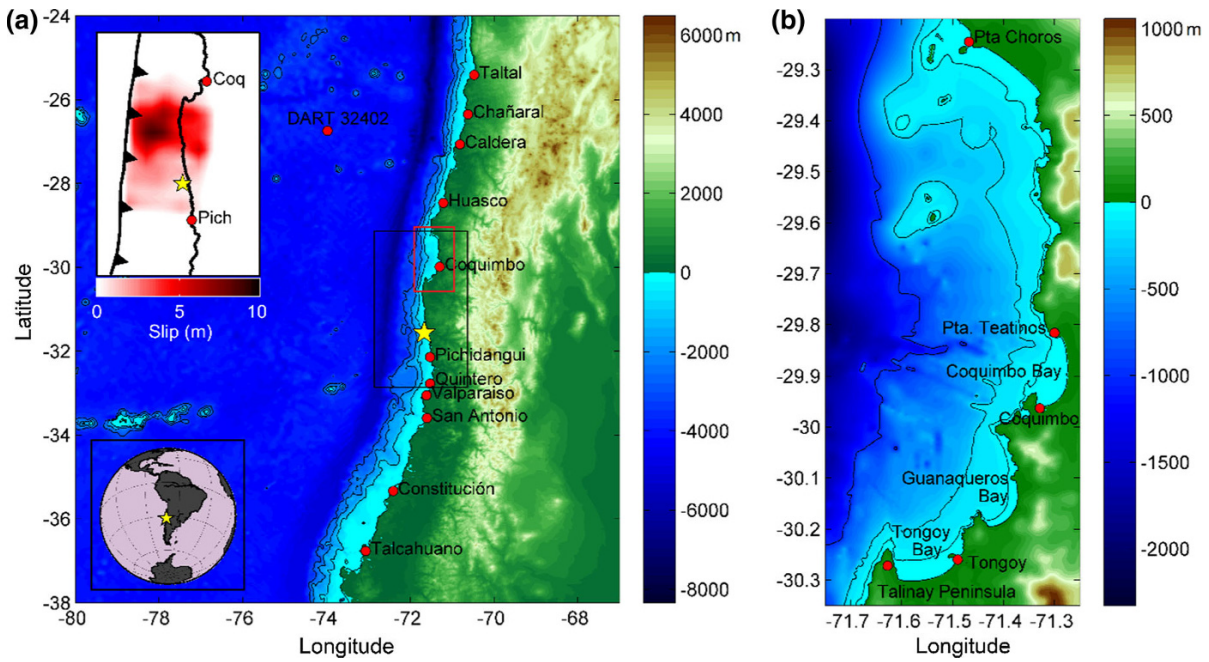

Figure 1

a Location of the tide gages and DART buoy. The *yellow* star indicates the epicenter and the thin *black lines* are the −1000, −2000 and −3000 m isobaths. *Upper inset* is the slip distribution of the 2015 Illapel earthquake. The *red* box is the enlarged area in the *right* frame. **b** Bathymetry in the area of interest. The thin *black lines* denote the −50, −200 and −1000 m isobaths

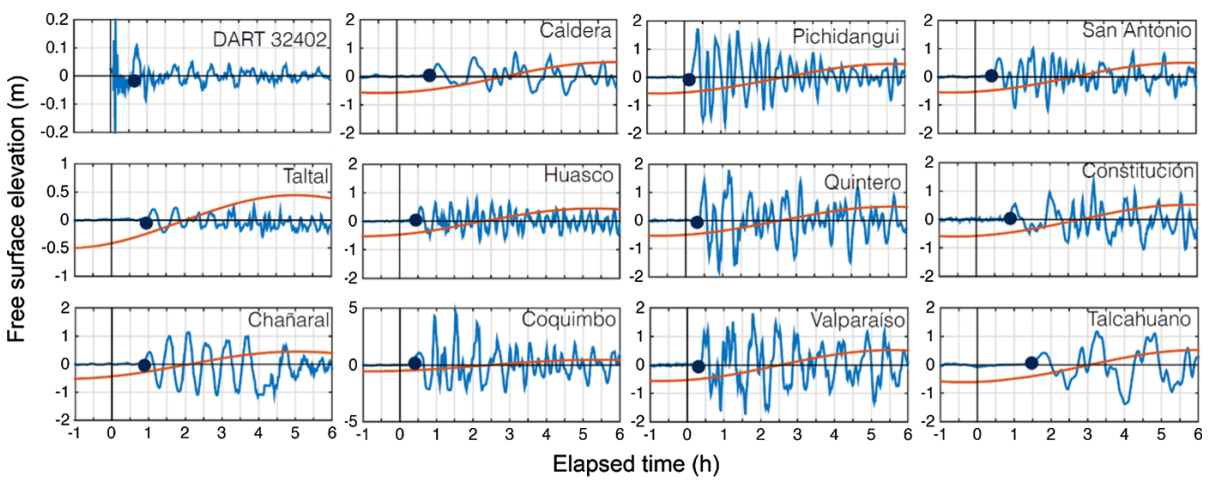

Figure 2

Tide gage records of the 2015 Illapel tsunami at locations indicated in Fig. 1a. The *red line* indicates the predicted tide level during the tsunami

wave, after which tsunami oscillations were persistent and periodic, but did not exceed 2 m in amplitude. About 100 km south of the rupture, the tsunami arrived at Quintero and Valparaiso within 23 min. The maximum amplitude of the first wave was 1.5 m, 30 min after the shock at Quintero and 1.22 m, 34 min after the shock at Valparaiso. However, the maximum amplitude at Valparaiso was

found to be much lower than at Coquimbo, reaching 1.90 m 108 min after the earthquake. Tide gage stations located farther north and south show a significant decrease in tsunami amplitude, with amplitude not exceeding 1 m. However, the behavior was noteworthy at Chañaral (26.32°S, 70.60 W) and Talcahuano (36.71°S, 73.11 W), where tsunami amplitudes were larger than stations located closer to the rupture patch, such as San Antonio and Constitución. Talcahuano was one of the most affected areas during the 2010 Chile tsunami (Fritz *et al.* 2011) and large amplification due to tsunami resonance has been identified (Yamazaki and Cheung 2011; Aranguiz 2015). This significant spatial variation of tsunami amplitudes at tide gage stations is consistent with the near-field behavior reported for the 2010 Maule and 2014 Pisagua tsunamis (Fritz *et al.* 2011; Catalan *et al.* 2015), and observed for the 2011 Tohoku far-field tsunami.

4. Post Tsunami Survey

Three different teams surveyed the area, recording tsunami runup, flow depth, inundation area and eyewitness testimonies. The field measurements were surveyed from the waterline in accordance with established post tsunami survey procedures (Dengler *et al.* 2003; Synolakis and Okal 2005; Dominey-Howes *et al.* 2012). The area is characterized by a microtidal regime of 2 m (Shoa 2015b), and data were corrected for tide level at the time of maximum inundation. Measurements were collected using both Kinematic Global Positioning System and laser rangefinders. All data measurements are given in Table 1 in "Appendix".

Figure 3 shows the runup and inundation height measurements. The highest measured runup of 10.8 m was found at the Totoral fishing village (30.365°S, 71.67°W), located immediately shoreward of the tsunami source area. The runup measured here was somewhat of an outlier relative to nearby measurements which were mostly in the 4–6 m range (Fig. 3a). The high runup at Totoral may be attributable to the deep offshore bathymetry and the pocket beach morphology that funneled the tsunami wave ashore. The tsunami penetrated over 200 m inland and washed away several wooden houses, leaving only their foundations (Fig. 4). According to local residents, at least five large waves flooded the bay in a slow manner, with an almost uniform inundation height in the whole bay. In addition, the first wave arrived a few minutes after the earthquake. As a proxy for first tsunami arrival time, Fig. 4c shows a clock found by the Chilean Navy at Totoral which stopped at 8:06 pm, arguably due to flooding, suggesting that the village may have been flooded 12 min after the initiation of the earthquake. However, doubts of the clock precision, the exact cause of clock malfunction put uncertainties around that arrival time estimate. Despite the short arrival time, only one person died due to the tsunami in Totoral Village. The body was found at Caleta Hornos, some 90 km north of Totoral (La Tercera 2015).

In general, it can be seen from Fig. 3a that the runup heights vary between 3 and 6 m at both sides of the rupture area with an asymmetric decaying trend. However, the runup and inundation heights show variable behavior along the southern section, where many small bays (such as Pichidangui and other bays south of Los Vilos) showed no significant tsunami traces. Damage was concentrated at Los Vilos, and Concon, 15 km north of Valparaíso. In both Los Vilos and Concon, runup reached $\sim$4 m. It was observed that damage was concentrated in the southern ends of these bays due to their being open to the north and thus receiving direct tsunami impact.

Similarly, we documented a high variability of the runup within Coquimbo, Guanaqueros and Tongoy Bays (Fig. 3b). For example, in Coquimbo Bay runup decreased progressively from west to east; on the western border the runup was 6.41 m, while in the middle section of the bay (near the tourist landmarks the Lighthouse and La Serena Golf Club) the runup was 3.31–2.98 m, respectively. A similar variation was observed in Tongoy Bay. In Puerto Aldea, located at the western border of the bay, runup reached 6.09 m, while Playa Grande at the western shore of Tongoy peninsula (eastern shore of Tongoy Bay) runup reached just 3.89 m. Interestingly, in Guanaqueros Bay runup at western and eastern shores were modest with only 3.26–2.61 m, respectively. Therefore, our data show that Coquimbo and Tongoy Bays experienced the largest runup at the

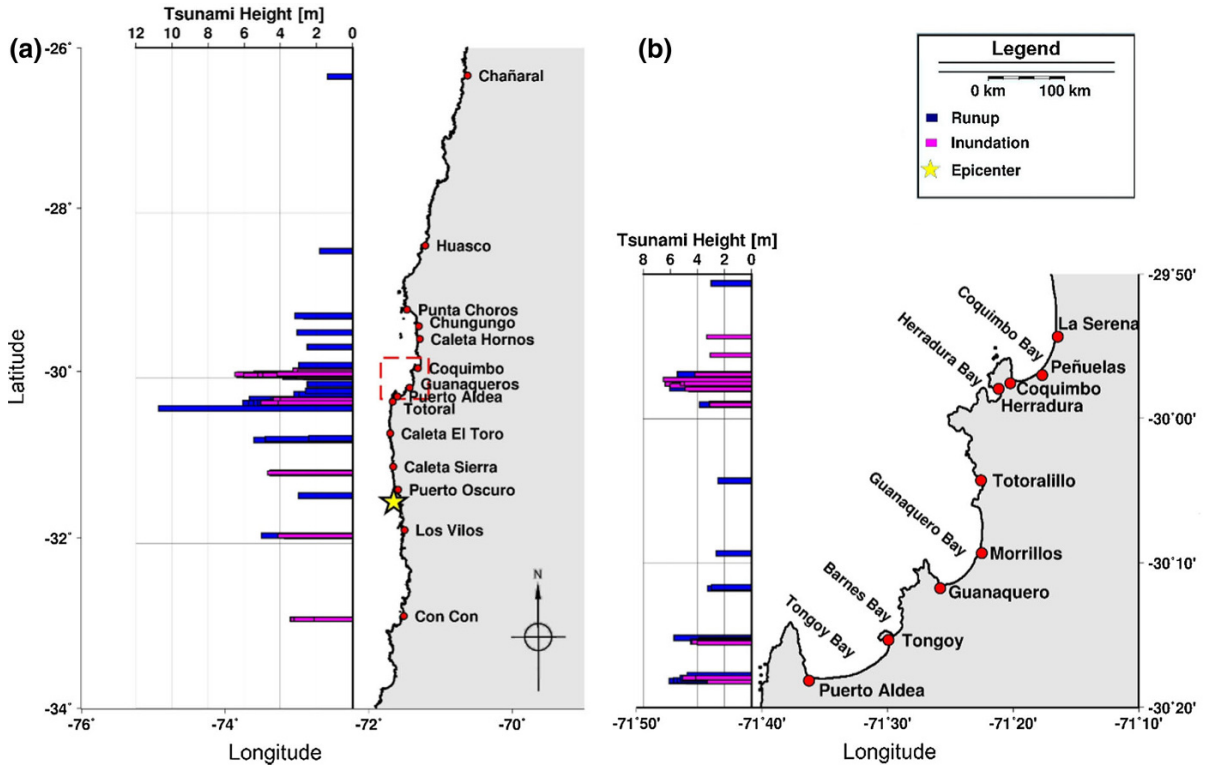

Figure 3
Results of the post tsunami survey. **a** Tsunami runup and inundation heights measured along 700 km of coastline from Chañaral to Concón. **b** Tsunami runup and inundation heights in the enlarged area

southwestern ends of their corresponding bays, while Guanaqueros Bay did not experience significant runup despite being located between the aforementioned two bays and having a similar orientation. One relevant aspect of the runup distribution is that these bays are located north of the main rupture area and are exposed to the north; each also has a peninsula on its western end. Therefore, they could have been somewhat sheltered from the main tsunami propagation path. In contrast, the area near Caleta Hornos, on the northern end of Coquimbo Bay and directly exposed to the main tsunami path, showed lower runup (2.5 m) and inundation.

As a result of this variability and the low density of dwellings in the area, damage was concentrated in specific locations. Figure 5 shows the inundation area of the three most affected locations, namely, Los Vilos, Tongoy and Coquimbo. Los Vilos is located south of the tsunami source area (Fig. 3), and the maximum tsunami height was 4.13 m. The beach is steeply sloped, relatively narrow (~70 m) and is backed by an almost vertical cliff at the southern end. Consequently, inundation extent was only about 150 m. Despite this, the tsunami inundated the first line of houses and in some cases drifting boats from the pier located at the southern end of the bay travelled to the northern side and caused significant destruction (Fig. 6a).

The greatest tsunami inundation distances were found in the north-facing bays of Coquimbo and Tongoy. In Coquimbo Bay we measured a maximum inundation distance of 700 m. Near this area of maximal tsunami penetration, tsunami waves overtopped the coastal road as well as a railway embankment, generating severe damage on the landward (Fig. 6c, d). The tsunami reportedly arrived from the north with at least three large waves. The number of waves were confirmed during the survey by the number of mudlines observed on sides of flooded houses (Fig. 6e). In the town of Tongoy,

Figure 4
Tsunami impact in Totoral. **a** Remnants of destroyed houses located along the southern shore of the Bay. **b** Estimated inundation area (source: Google Earth). The *green triangle* indicates the measured runup. **c** Clock found at Totoral with time indicating the arrival of the first flooding

maximum inundation reached 600 m inland, temporarily isolating the Tongoy Peninsula as an offshore island, an effect also reported—albeit at much larger scale—at the northern tip of Sumatra Island during the 2004 Indian Ocean tsunami (Borrero 2005). In this locality, the maximum runup was 5.72 m, with a very narrow inundation extent, indicative of splashing up, near the eastern shore of the peninsula (Fig. 5) while it was 4.51 m in the town. As mentioned earlier, runup at the western shore of the peninsula reached only 3.89 m. Despite the large inundation height, due to the topography the flow depth ranged between just 1 to 2 m (Fig. 6b).

To better explain the tsunami inundation pattern at Coquimbo, the transect A–A was measured and indicated in the lowest panel of Fig. 5. The measurements along the transect demonstrated that the inundation height was almost uniform and bounded by a vertical retaining wall (an image of the retaining wall is given in Fig. 6f). It was found that the urbanized area on the leeside of the railway had a ground elevation of approximately 3 m (see transcect A–A in Fig. 5), which is lower than the coastal road and railway elevations. It is important to mention that the railway decreases in height as it approaches the coast westward while at the wetland it gets narrower

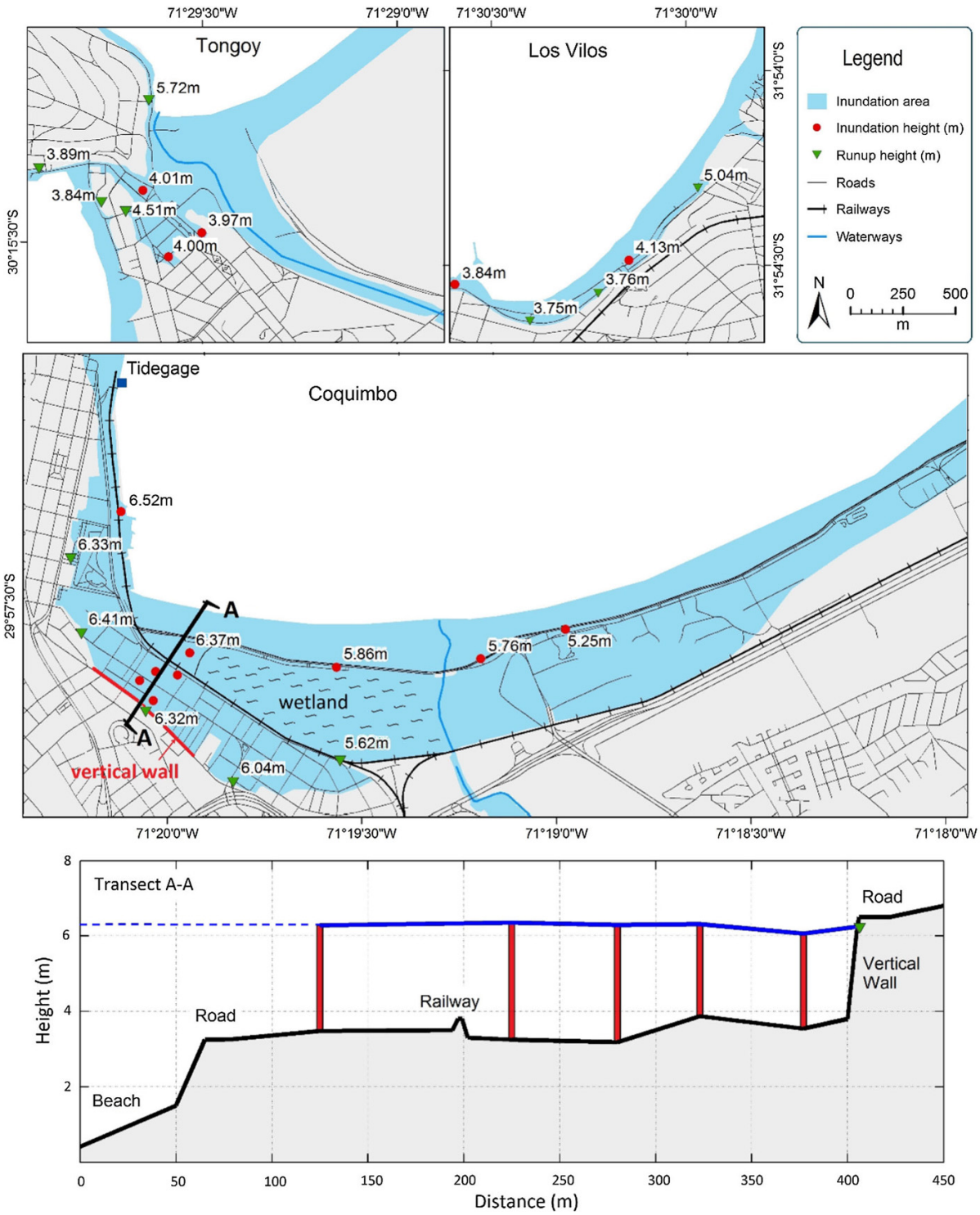

Figure 5
Inundation area at Tongoy, Los Vilos and Coquimbo. The *lower panel* shows a transect of the inundation profile at Coquimbo

Figure 6
a Seaweed and tsunami debris in a fence at Los Vilos. **b** Water mark on a wooden house in Tongoy. **c** Damage on the coastal road in Coquimbo due to tsunami overtopping. **d** Damage on the railway at Coquimbo. **e** Several water marks on a masonry house at Coquimbo. **f** Retaining wall in Coquimbo

and the distance between the shore and the vertical wall decreases. Subsequently, all the mentioned factors contributed to funneling the incoming tsunami and increasing the inundation depth and runup compared to sections a few hundred meters east.

Finally, along the coast of Talinay, south of Totoral to Puerto Oscuro, the tsunami runup gradually decreased with tsunami inundation distance typically of a few tens of meters (Fig. 3). An exception occurred at the Limari River (40 km south of Totoral) where tsunami penetrated 3.95 km upriver with a runup of 3 m.

5. Numerical Simulation

To better understand the tsunami runup distribution, arrival time and other effects such as the seafloor

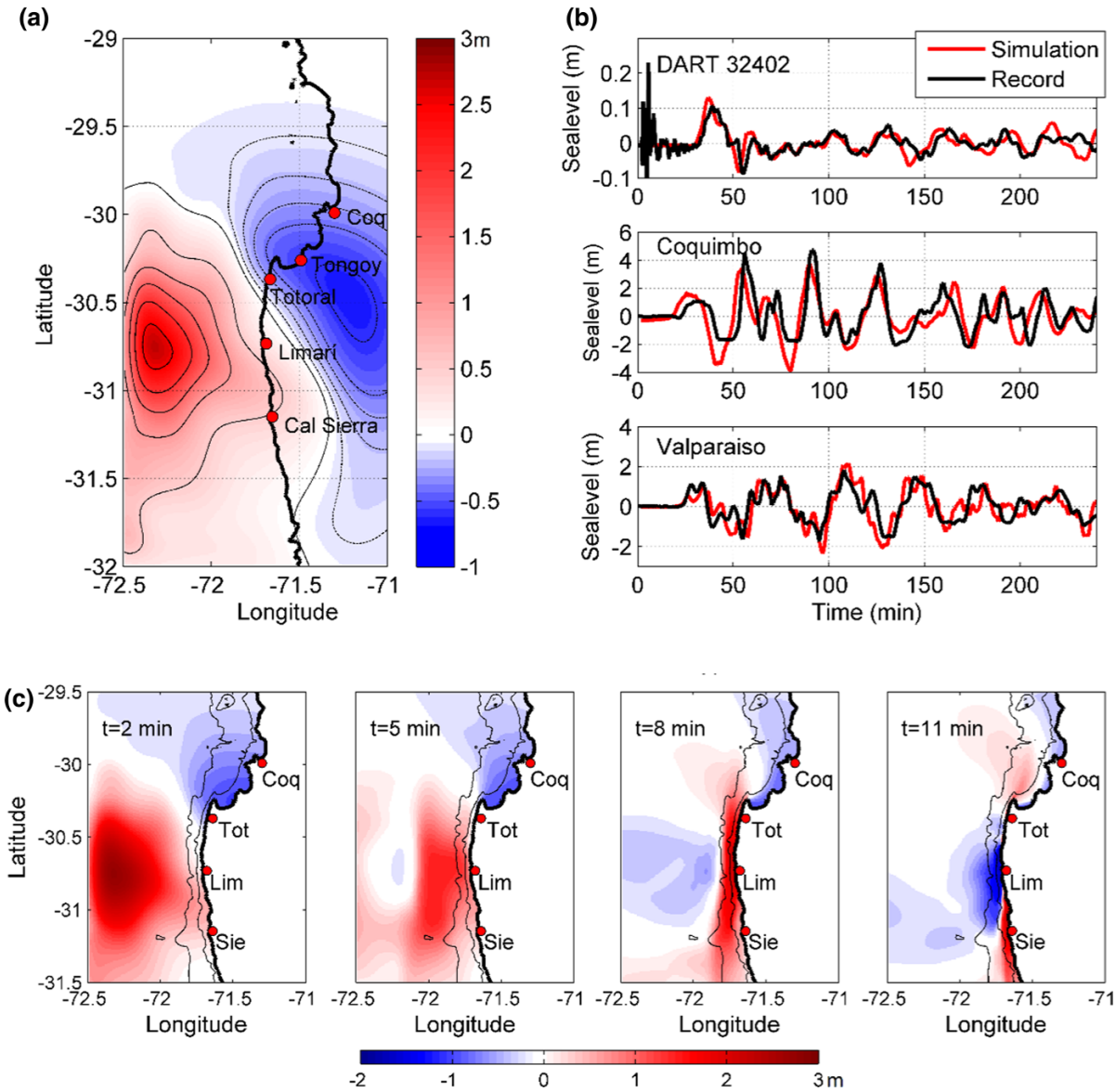

Figure 7

Results of numerical simulation. **a** Vertical displacement, *red* area is uplift while *blue* is subsidence. *Continuous lines* are uplift at 0.5 m intervals, and *dashed lines* denote subsidence at 0.1 m intervals. **b** Modeled and measured tsunami waveforms at DART32402, Coquimbo and Valparaiso. **c** Snapshots of tsunami propagation, the *black lines* denote the −1000 and −200 m isobaths

vertical displacement, we performed a tsunami numerical simulation by means of the NEOWAVE model (Yamazaki *et al.* 2009, 2011). The tsunami was simulated using 3 levels of nested grids with resolutions of 120″(∼3.6 km), 30″(∼900 m) and 6″(∼180 m). The level 1 grid was built from GEBCO bathymetric data, while the level 2 and 3 grids also considered nautical charts from SHOA. The level 3 grid covered all bays from 29.1°S in the north to 30.5°S in the south. The tsunami initial condition was obtained from the Okada (1985) formulation with the finite fault model of the rupture area of variable slip given in Fig. 1. We used a 200 km by 200 km region with 400 subfaults of

10 km by 10 km each. The fault model considered constant strike, dip and rake angles of 5°, 15° and 117°, respectively, consistent with the slab geometry in the area.

The maximum slip was computed to be 8.62 m and was located north of the epicenter (Fig. 1). Figure 7a shows the level 2 grid and the vertical displacement of the sea floor. The maximum uplift was found to be 2.7 m offshore from the mouth of the Limarí River, while the model suggests that Coquimbo, Guanaqueros, and Tongoy Bays experienced subsidence between 30 and 45 cm. Furthermore, we computed the mean water level from the Coquimbo tide gage before and after the tsunami from online data (www.ioc-sealevelmonitoring.org) and the results showed a subsidence of 7–10 cm due to the earthquake. For validation of the numerical model, we used three records, namely the DART buoy 32402, and the tide gages at Coquimbo and Valparaiso (Fig. 1). The numerical simulation of Valparaiso considered four levels of nested grids of $120''(\sim 3.6$ km), $30''(\sim 900$ m), $6''(\sim 180$ m), and $1''(\sim 30$ m) resolution. In all cases, the computation considered 4 h of elapsed time and output interval of 10 s. The free surface elevation time series are shown in Fig. 7b. A good agreement between the simulation and records is seen considering both arrival time and maximum amplitude, although the simulation produces tsunami arrivals 3–5 min earlier at Coquimbo. Figure 7c shows snapshots of the tsunami propagation where it can be observed that the first tsunami wave arrived to the Talinay Peninsula 8 min after the initiation of the earthquake. In addition, the tsunami continues to propagate into the Coquimbo Bay after 11 min, while the first ebb is already taking place along the coast between Totoral fishing village and Limarí river mouth.

Figure 8 shows the maximum tsunami runup along the coast obtained from the level 2 and 3 grids. In general, it can be seen that the numerical simulation is in good agreement with the measurements. However, the maximum runup at Totoral is underestimated by the model. A possible reason for this is the relatively coarse modeling grid (~ 180 m) as compared to the entrance of the bay which was only ~ 500 m across. Figure 8 shows that modeled tsunami runup ranged from 2 to 6 m and resolved the runup peaks at Los Vilos and Coquimbo Bay to the south and north of the epicenter.

6. Discussion

The tide gage data shows that the tsunami arrived quickly after the earthquake. The first tsunami wave reached a maximum amplitude of 1.8 m 20 min after the main shock at Pichidangui, and 1.1 m after 30 min at Coquimbo. These values are in good agreement with previously reported arrivals times during the 2010 Maule earthquake and tsunami (Larrañaga 2010; Fritz *et al.* 2011). However, a close view of the coastal area of Talinay, which is located in front of the rupture, shows that this area experienced much shorter arrival times. For example, the Totoral fishing village eyewitness accounts and stopped clock evidence suggest possible arrival even earlier than 12 min. That evidence is corroborated by the tsunami modeling results. The closeness of the main rupture patch to the coast as well as the very narrow continental shelf and steep bathymetry allowed a rapid propagation of the tsunami toward the coast. This short tsunami arrival time put the tsunami awareness of coastal residents in Chile to the test. However, it must be noted that the area located just in front of the rupture is known for having a low population density, and that the event occurred in the evening, after the end of the work day, and during the tourism off-season.

An interesting feature of the tsunami related to the 2015 Illapel earthquake was its regionally asymmetric tsunami height distribution with respect to the source region. Our field data showed that runup decayed at a shorter distance to the north relative to the south of the rupture. These results are in good agreement with the numerical simulations, which reproduced most of the local observations. The lack of high-resolution bathymetric data and seismic source uncertainties may explain the observed mismatch between measured and modeled water levels. In that regard, the regional scale asymmetry of tsunami parameters can be explained by the bathymetric configuration. Figure 1 shows that slope of the sea bottom is gentler to the south of the source area compared to the north. The gentler slope in the south

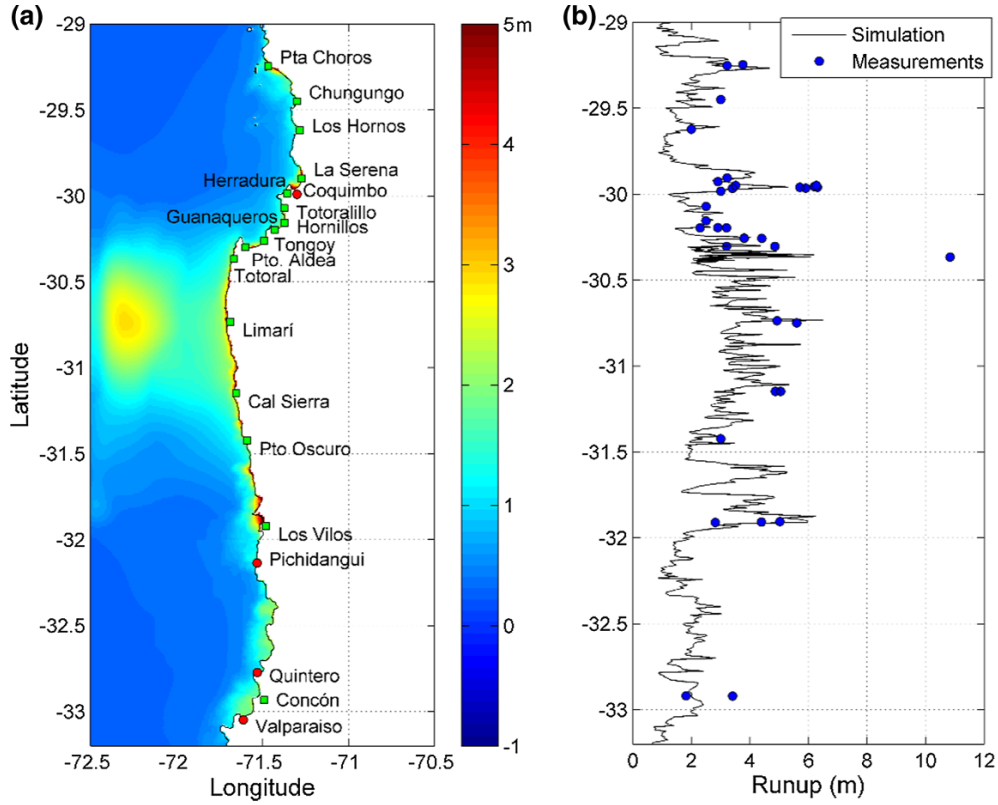

Figure 8
a Maximum tsunami amplitudes from the numerical simulation. **b** Comparison of tsunami height measurements and numerical simulation

can also affect resonance processes controlling the observed slower decay of runup in the south with respect to the northern section. As with other recent tsunamis in Chile (Fritz *et al.* 2011; Yamazaki and Cheung 2011; Catalan *et al.* 2015), both the runup distribution and the phase of the maximum wave varied considerably along the coast and seemed to be significantly influenced by coastal morphology and bathymetry. Local morphology plays a major role and the analysis of tsunami hydrodynamics should be studied in more detail. In addition, the rocky coastal cliffs, the relatively steep bathymetries and narrow bays oriented directly along the main tsunami propagation path could funnel tsunami energy, which would explain the high runup observed at Totoral. Nevertheless, a similar situation may have occurred at other places near the source of the tsunami, but the low population density in the area, limited road access to the coast and the lack of vegetation prevented more traceable tsunami inundation evidence from being found.

The 2015 event is comparable to the 2014 Pisagua event in terms of magnitude, but the different response of the tsunami is noteworthy. For the 2014 event, maximum runup did not exceed 4 m, whereas for this event runup in the 4 m range was typical with values exceeding 6 m at several locations as well as the maximum of 10.8 m at Totoral. Consequently, the magnitude of the earthquake is not sufficient to explain these differences. Models of the co-seismic slip distribution for these events (i.e. Hayes 2014; Okuwaki *et al.* 2015, this issue) suggest that the bulk of the seismic slip from the 2015 Illapel earthquake occurred at much shallower depths as compared to the 2014 Pisagua event resulting in a relatively larger initial tsunami amplitude. For this event, initial tsunami heights were of the order of 2.5 m whereas Catalán *et al.* (2015) modeled initial tsunami heights

of <2.0 m from the Pisagua event using the slip distribution model of An *et al.* (2014). Hence the initial tsunami energy was significantly larger for this event and is likely the result of the relatively shallowness of the rupture, as suggested by Geist (2002).

As we mentioned above, the April 1943 event was the last significant earthquake in the area, and was estimated at Mw 8.3 by Lomnitz (1970), although Beck *et al.* (1998) revised this to Mw 7.9 based on their undiffracted teleseismic P-waves. However, tsunami reports suggest just a minor tsunami impact at Los Vilos and no tsunami inundation in Coquimbo (Lomnitz 1970; Soloviev and Go 1975). This tsunami arrived at Valparaiso 22.3 min after the earthquake, which is a time similar to the present observations (Figs. 2, 7). However, its initial tsunami amplitude was just 80 cm (Soloviev and Go 1975). The analyses and data presented here indicate that the 2015 tsunami is markedly different from the tsunami from the 1943 event suggesting differences in the earthquakes' magnitude, location and/or slip distribution.

7. Conclusions

A field survey after the September 16 earthquake and tsunami recorded valuable data on the tsunami impact. Tsunami runup from this event was generally between 4 and 6 m near the source region with a maximum of 10.8 m. This area was previously impacted by a similarly sized tsunamigenic earthquake in 1943, although the tsunami generated by that event was much smaller than the present day event. An asymmetric variation of tsunami height was observed to the north and south of the earthquake epicenter, while the runup and phase of the maximum wave also varied considerably along the coast. Furthermore, it was evident that local bathymetric and topographic features caused a remarkable effect on tsunami amplification and the most significant tsunami damage was concentrated in just a few developed coastal areas. When compared to the recent, similarly sized, April 2014 Pisagua earthquake and tsunami in northern Chile, runup from this event was consistently larger and was likely a result of the shallow nature of co-seismic slip distribution as compared to the 2014 event. In terms of public safety and hazard mitigation, arrival times for the 2015 tsunami were found to be <12 min at the closest coastal villages, in contrast to other near-field tsunamis along the Chilean margin. However, the low number of casualties can be explained by the general tsunami awareness and self- evacuation efforts among local residents as well as the low population density along the affected area. However, the short arrival time of the first inundation, as reported by witnesses and confirmed by numerical modeling, should warrant further discussion about public priorities and investments in hazard mitigation that earthquake and tsunami prone countries must undertake to reduce casualties due to future tsunamis.

Acknowledgments

The authors would like to thank CONICYT (Chile) for its FONDAP 15110017, and FONDECYT 11140424 grants as well as FB0821 grant. Thanks to the Faculty of Engineering at UCSC for the partial funding of the post tsunami survey. The authors also thank The Japan International Cooperation Agency (JICA) and the Japan Science and Technology Agency (JST) through their SATREPS Program "Enhancement of Technology to Develop Tsunami-resilient Community". Special thanks to people who contributed to the collection of field data: Stephane Abadie, Patricio Winckler, Jose Baquedano, Matias Carvajal, Pablo Cortes, Alejandra Gubler, Raimundo Ibaceta, Cyril Mokrani, Alejandro Urrutia, Georgette Mell, Carlos Inostroza, Bob Keulers and Kimberley Koudstaal. Thanks to the Chilean Navy and the Municipality of Coquimbo for their important help during the field survey. We thank the editor and the two reviewers for their comments which help us to improve the manuscript.

Appendix

See Table 1.

Table 1

Tsunami dataset recorded in Chile from 21 September to 1 November 2015

No.	Location	Description	E	N	Inundation/runup height (m)	distance from shore (m)	Inundation or runup	Measured time (local)	Marks
1	Coquimbo	Palm tree	−71.31990	−29.96036	5.71	156	I	9-22-2015 10:30	Algae
2	Coquimbo	Building	−71.33236	−29.96015	6.37	150	I	9-22-2015 10:35	Water mark
3	Coquimbo	Street	−71.33700	−29.95944	6.41	238	R	9-22-2015 10:38	Sand, brown vegetation
4	Coquimbo	Bus terminal	−71.33746	−29.95667	6.33	221	R	9-22-2015 10:45	Sand, eyewitness
5	Coquimbo	Parking place	−71.33051	−29.96495	6.04	634	R	9-22-2015 10:48	Brown vegetation
6	Coquimbo	Palm tree	−71.32607	−29.96068	5.86	149	I	9-22-2015 10:51	Algae
7	Coquimbo	Building	−71.33530	−29.95491	6.52	26	I	9-22-2015 10:58	Water mark
8	Coquimbo	House	−71.33245	−29.96221	6.02	380	I	9-22-2015 11:03	Water mark
9	Coquimbo	Building	−71.33277	−29.96097	6.44	248	I	9-22-2015 11:11	Water mark
10	Coquimbo	Building	−71.33383	−29.96101	6.38	275	I	9-22-2015 11:18	Water mark
11	Coquimbo	House	−71.33470	−29.96123	6.42	334	I	9-22-2015 11:23	Water mark
12	Coquimbo	House	−71.33419	−29.96191	6.15	380	I	9-22-2015 11:31	Water mark
13	Coquimbo	Wall	−71.33440	−29.96198	6.33	401	R	9-22-2015 11:43	Water mark
14	Peñuelas	House	−71.29542	−29.94962	3.60	109	I	9-23-2015 18:30	Water mark
15	Peñuelas	Fence	−71.29467	−29.95011	3.69	203	I	9-23-2015 18:31	Water mark
16	Tongoy	Public toilet	−71.49418	−30.25644	4.01	320	I	9-23-2015 10:30	Water mark
17	Tongoy	Street	−71.49395	−30.25310	5.72	32	R	9-23-2015 10:36	Sand, brown vegatation
18	Tongoy	House	−71.49519	−30.25604	3.68	340	I	9-23-2015 10:39	Water mark
19	Tongoy	Retaining wall	−71.49866	−30.25563	3.89	47	R	9-23-2015 10:45	Water mark
20	Tongoy	Street	−71.49599	−30.25687	3.84	83	R	9-23-2015 10:48	Eyewitness
21	Tongoy	Street	−71.49495	−30.25722	4.51	441	R	9-23-2015 10:54	Eyewitness
22	Tongoy	Wall	−71.49168	−30.25799	3.97	474	I	9-23-2015 11:03	Water mark
23	Tongoy	House	−71.49365	−30.25721	3.90	401	I	9-23-2015 11:10	Water mark
24	Tongoy	House	−71.49399	−30.25795	4.39	490	I	9-23-2015 11:18	Water mark
25	Tongoy	House	−71.49311	−30.25888	4.00	580	I	9-23-2015 11:32	Water mark
26	Guanaquero	Parking	−71.43005	−30.19609	3.26	31	R	9-23-2015 15:00	Algae
27	Guanaquero	Fence	−71.42955	−30.19581	2.43	31	R	9-23-2015 15:01	Algae
28	Guanaquero	Quey platform	−71.43085	−30.19468	2.96	31	R	9-23-2015 15:02	Eyewitness
29	Morrillos	Beach	−71.37489	−30.15554	2.61	82	R	9-23-2015 16:30	Algae
30	Chungungo	Beach	−71.30363	−29.45002	3.07	16	R	9-24-2015 17:15	Algae
26	Los Hornos	Quay	−71.28863	−29.62251	2.50	10	R	9-24-2015 16:30	Eyewitness
27	Puerto Oscuro	Beach	−71.59267	−31.42310	3.00	56	I	9-25-2015 9:30	Brown vegetation
28	La Serena	Lighthouse	−71.27409	−29.90567	3.31		I	31-10-2015 17:24	Water mark
29	La Serena	4 esquinas	−71.27860	−29.92683	3.06		I	31-10-2015 17:57	Water mark
30	Herradura	Fence	−71.35369	−29.98246	3.12		I	31-10-2015 19:00	Algae
31	Herradura	UCN pier	−71.35248	−29.96594	4.36		R	31-10-2015 20:07	Eye witness
32	Puerto Aldea	Factory	−71.58381	−30.30368	3.28		I	01-11-2015 11:13	Water mark
33	Puerto Aldea	Road	−71.60406	−30.30253	4.96		R	01-11-2015 10:20	Algae, debris, brown vegetation

Table 1 *continued*

No.	Location	Description	E	N	Inundation/runup height (m)	distance from shore (m)	Inundation or runup	Measured time (local)	Marks
34	Totoralillo	Beach	−71.37583	−30.07175	2.50		R	01-11-2015 9:30	Algae, debris
35	Caleta Sierra	Beach	−71.66023	−31.14807	4.57		R	07-10-2015 13:10	Algae and debris
36	Caleta Sierra	Beach	−71.66165	−31.14708	4.71		I	07-10-2015 12:57	Flooding mark
37	Limari	Rocky beach	−71.70296	−30.74859	5.47		R	24-09-2015 13:14	Algae and debris
38	Limari	Rocky beach	−71.70160	−30.73657	4.84		R	24-09-2015 15:30	Algae and debris
39	Limari	River bank	−71.658537	−30.729330	3.03	3950	R	25-09-2015 15:30	Brown vegetation
40	Totoral	Beach	−71.66751	−30.36585	10.75	210	R	25-09-2015 17:42	Algae and debris
41	Puerto Aldea	Beach	−71.60204	−30.30309	4.79		R	23-09-2015 18:47	Algae and debris
42	Puerto Aldea	Beach	−71.60603	−30.30270	6.09		R	23-09-2015 19:05	Algae and debris
43	Puerto Aldea	Beach	−71.60324	−30.30271	4.77		R	23-09-2015 18:52	Algae and debris
44	Puerto Aldea	Beach	−71.60406	−30.30238	4.84		R	23-09-2015 18:54	Algae and debris
45	Puerto Aldea	Beach	−71.60496	−30.30228	5.76		R	23-09-2015 18:56	Algae and debris
46	Puerto Aldea	Beach	−71.60527	−30.30216	5.48		R	23-09-2015 18:57	Algae and debris
47	Puerto Aldea	Beach	−71.60774	−30.29978	5.19		R	23-09-2015 16:53	Algae and debris
48	Puerto Aldea	Beach	−71.60790	−30.29937	5.09		I	23-09-2015 16:55	Flooding mark
49	Puerto Aldea	Beach	−71.60800	−30.29931	5.25		R	23-09-2015 16:57	Algae and debris
50	Puerto Aldea	Beach	−71.60765	−30.29906	4.12		I	23-09-2015 17:01	Flooding mark
51	Puerto Aldea	Beach	−71.60799	−30.29616	4.76		R	23-09-2015 17:17	Algae and debris
52	Golf La Serena	Beach	−71.27899	−29.84402	2.98		R	26-09-2015 10:47	Sand and debris
53	Cal. Herradura	Beach	−71.36326	−29.98430	2.71		R	08-10-2015 11:44	Sand and debris
54	Cal. Herradura	Beach	−71.36324	−29.98414	3.09		I	08-10-2015 11:45	Flooding mark
55	Cal. Herradura	Beach	−71.36538	−29.98388	3.85		R	08-10-2015 11:40	Sand and debris
56	Herradura	UCN Pier	−71.35249	−29.96597	4.92		I	08-10-2015 12:29	Flooding mark
57	Herradura	UCN Pier	−71.35251	−29.96587	4.62		R	08-10-2015 12:29	Sand and debris
58	Coquimbo	Beach	−71.31691	−29.96013	4.50		I	08-10-2015 10:58	Flooding mark
59	Coquimbo	Beach	−71.31628	−29.95969	5.25		I	08-10-2015 10:48	Flooding mark
60	Coquimbo	Beach	−71.31642	−29.95967	4.97		I	08-10-2015 10:46	Flooding mark
61	Capitania Coq	Square	−71.33690	−29.94911	4.19		I	08-10-2015 13:30	Flooding mark
62	Capitania Coq	Square	−71.33721	−29.94905	5.47		R	08-10-2015 13:31	Sand and debris
63	Playa Conchita	Beach	−71.44226	−29.25243	2.70		R	26-09-2015 15:12	Sand and debris
64	Punta Choros	Pier	−71.46814	−29.24696	3.21	37	R	26-09-2015 16:08	Flooding mark
65	Huasco	Beach	−71.21411	−28.46208	1.83	28	R	26-09-2015 20:18	Flooding mark
66	Chañaral	Beach	−70.62475	−26.34549	1.39	151	R	27-09-2015 9:03	Flooding mark
67	Chañaral	Beach	−70.62488	−26.34522	1.39	151	R	27-09-2015 9:04	Flooding mark
68	Chañaral	Beach	−70.62529	−26.34478	1.38	151	R	27-09-2015 9:05	Flooding mark
69	Concón	Wall	−71.51301	−32.92082	2.59	98	I	9-17-2015 12:22	Watermark
70	Concón	Trailer	−71.51292	−32.92029	3.46	55	I	9-17-2015 13:09	Watermark
71	Concón	Restaurant	−71.51293	−32.92078	3.46	102	I	9-17-2015 13:09	Watermark
72	Concón	House	−71.51101	−32.91942	3.43	83	I	9-17-2015 13:40	Watermark
73	Concón	Watermark	−71.51076	−32.91954	3.25	104	I	9-17-2015 13:40	Watermark
74	Concón	Rock	−71.50901	−32.91935	2.14	218	I	9-17-2015 14:05	Watermark

Table 1 *continued*

No.	Location	Description	E	N	Inundation/runup height (m)	distance from shore (m)	Inundation or runup	Measured time (local)	Marks
75	Los Vilos	House	−71.50015	−31.90578	3.50	54	I	9-22-2015 10:26	Water mark
76	Los Vilos	Street	−71.50115	−31.90685	3.86	86	R	9-22-2015 10:46	Marks on grass
77	Los Vilos	Alley	−71.50541	−31.91064	3.76	63	R	9-22-2015 11:54	Algae
78	Los Vilos	Street	−71.50667	−31.91072	3.75	65	R	9-22-2015 12:02	Algae
79	Los Vilos	Fishermen's cove	−71.50987	−31.90915	3.84	75	I	9-22-2015 12:40	Water mark
80	Los Vilos	House	−71.49952	−31.90534	4.13	96	I	9-22-2015 10:13	Eyewitness
81	Los Vilos	House	−71.50073	−31.90633	3.38	58	I	9-22-2015 10:34	Water mark
82	Los Vilos	Street	−71.50106	−31.90695	5.04	90	R	9-22-2015 10:52	Eyewitness
83	Los Vilos	Wall	−71.50286	−31.90885	4.13	91	I	9-22-2015 11:35	Water mark

References

An, C.; Sepúlveda, I. & Liu, P. L.-F. (2014), *'Tsunami Source and Its Validation of the 2014 Iquique, Chile Earthquake'*, Geophysical Research Letters *41*(11), 3988–3994, doi: 10.1002/2014GL060567

Aránguiz, R., (2015). *Tsunami Resonance in the Bay of Concepción (Chile) and the effect of Future Event*. Handbook of Coastal Disaster Mitigation for Engineers and Planners. http://dx.doi.org/10.1016/B978-0-12-801060-0.00006-X

Beck, S., Barrientos, S., Kausel, E., Reyes M., (1998). *Source characteristics of the historic earthquake along the central Chile subduction zone*. Journal of South American Earth Science, Vol *11* No 2 pp 115–129.

Borrero, J.C. (2005). *Field Data and Satellite Imagery of Tsunami Effects in Banda Aceh*, Science, V. *308*, p. 1596 June 10, 2005.

Catalán, P., Aránguiz, R., González, G., Tomita, T., Cienfuegos, R., González, J., Shrivastava, M., Kumagai, K., Mokrani, C., Cortés, P., Gubler, A., (2015), *The 1 April 2014 Pisagua tsunami: Observations and modeling*, Geophys. Res. Lett., *42*, doi:10.1002/2015GL063333

Dengler, L.; Borrero, J.; Gelfenbaum, G.; Jaffe, B.; Okal, E.; Ortiz, M.; Titov, V.; Anima, R.; Anticona, L. B.; Araya, S.; Gomer, B.; Gómez, J.; Koshimura, S.-i.; Laos, G. & Ocala, L. (2003), *'Tsunami'*, Earthquake Spectra *19*(S1), 115—144, doi: 10.1193/1.1737247

Dominey-Howes, D.; Dengler, L.; Dunbar, P.; Kong, L.; Fritz, H.; Imamura, F.; McAdoo, B.; Satake, K.; Yalciner, A.; Yamamoto, M.; Yulianto, E.; Koshimura, S. & Borrero, J. (2012), *'Post-Tsunami Survey Field Guide, 2nd Edition.'*(IOC Manuals and Guides No. 37), Technical report, UNESCO, Paris.

Fritz, H. M., Petroff, C. M., Catalán, P. A., Cienfuegos, R., Winckler, P., Kalligeris, N., Weiss, R., Barientos, S., Meneses, G., Valderas, C., Ebeling, C., Papadopoulus, A., Contreras, M., Almar, R., Dominguez, J. C., & Synolakis, C. E., (2011) *"Field Survey of the 27 February 2010 Chile Tsunami"*, Pure and Applied. Geophysics. Springer Basel AG.

Geist, E. (2002), *'Complex earthquake rupture and local tsunamis'*, Journal of Geophysical Research *107*(B5), 2086, doi: 10.1029/2000JB000139.

Hayes, (2014). *Preliminary Finite Fault Results for the Apr 01, 2014 Mw 8.2 99 km NW of Iquique*, Chile Earthquake (Version 1). [Available at: http://earthquake.usgs.gov/earthquakes/eventpage/usc000nzvd#scientific_finitefault].

La Tercera (2015). [http://www.latercera.com/noticia/nacional/2015/09/680-648455-9-terremoto-encuentran-cuerpo-de-mujer-en-coquimbo.shtml].

Larrañaga Martin, E. (2010), Analisis del Proceso de Toma de Decisiones, Fiscal de la Investigación Técnica, Armada de Chile, Valparaiso, Chile.

Lomnitz, C., (1970). *Major Earthquakes and Tsunami in Chile during the period 1535 to 1955*. Geol. Rundschau *59* (3), 938–960.

Nishenko, S.P., (1985). *Seismic potential for large and great interplate earthquakes along the Chilean and southern Peruvian margins of South America: a quantitative reappraisal.* J. Geophys. Res. *90*. http://dx.doi.org/10.1029/JB090iB05p03589. issn:0148-0227.

Okada, Y., (1985) *"Surface Deformation of Shear and Tensile Faults in a Half-Space"*, Bulletin of the Seismological Society of America, *75*, [4], 1135–1154.

Okuwaki, R., Yagi, Y., Aránguiz, R., González, J., González, G., (2015). *Rupture process during the 2015 Illapel, Chile earthquake: Zigzag-along-dip rupture episodes*, submitted to Pure Appl. Geophys., on 30 November 2015, for the special issue "2015 Chile".

ONEMI, (2015). Monitoreo por sismo de mayor intensidad. (In Spanish) [Available at: http://www.onemi.cl/alerta/se-declara-alerta-roja-por-sismo-de-mayor-intensidad-y-alarma-de-tsunami/].

SHOA, 2015a, Informe Preliminar Evento de Illapel, Servicio Hidrográfico y Oceanográfico de la Armada de Chile, 2015 (in Spanish)

SHOA, 2015b, Tablas de Marea de las Costas de Chile, Servicio Hidrográfico y Oceanográfico de la Armada de Chile, 2015 (in Spanish)

Soloviev, S.L., & Go, Ch., N., (1975) *"A catalogue of tsunamis on the Eastern shore of the Pacific Ocean"*, Nauka Publishing House, Moscow, 202p

Synolakis, C. & Okal, E. (2005), 1992–2002: Perspective on a Decade of Post-Tsunami Surveys, in K. Satake, ed., 'Tsunamis: Case Studies and Recent Developments', Springer, pp. 1–29.

Yagi, Y., and Fukahata, Y. (2011), *Introduction of uncertainty of Green's function into waveform inversion for seismic source processes*. Geophysical Journal International, *186* (2): 711-720.

Yamazaki, Y., and Cheung, K. F. (2011) *"Shelf Resonance and Impact of Near-field Tsunami generated by the 2010 Chile Earthquake"*, Geophyical Research Letters, *38*(12), L12605, doi: 10.1029/2011GL047508

Yamazaki, Y., Kowalik, Z., and Cheung, K. F. (2009) *"Depth-integrated, non-hydrostatic model for wave breaking and runup"*, Int. J. Numer. Methods Fluids, *61*(5), 473–497.

Yamazaki, Y., Cheung, K.F., and Kowalik, Z. (2011) *"Depth-integrated, non-hydrostatic model with grid nesting for tsunami generation, propagation, and runup"*. International Journal for Numerical Methods in Fluids, *67*(12), 2081–2107.

Ye, L., Lay, T., Kanamori, H., Koper, K., (2015). *Rapidly Estimated Seismic Source Parameters for the 16 September 2015 Illapel, Chile Mw 8.3 Earthquake*. Pure Appl. Geophys. doi: 10.1007/s00024-015-1202-y

(Received November 23, 2015, revised December 3, 2015, accepted December 7, 2015, Published online December 28, 2015)